Soft Matter

PAPER

View Article Online
View Journal | View Issue

Cite this: *Soft Matter*, 2025, 21, 3393

A cofactor mediated supramolecular oligo-adenine triplex for reprogrammable macroscopic hydrogel assembly†

Alycia Zi Ting Lim,‡[ab] Michael Shao Min Ho,‡[ac] Yujie Ke,[d] Wei Wei Loh,[a] Zhaogang Dong,[ae] Fuke Wang,[a] Jason Y. C. Lim,[a] Xin Ting Zheng,[a] Le Yang[a] and Yuwei Hu*[a]

Noncanonical DNA structures mediated by low-molecular-weight cofactors significantly enrich the arsenal of the DNA toolbox and expand its functional applications. In this study, cyanuric acid (CA), a cofactor with three thymine-like edges, is employed to assemble adenine-rich strands (A-strands) into a parallel noncanonical A-CA triplex configuration through Watson–Crick and Hoogsteen interactions. This assembly occurs at a system pH value below the pK_a of the CA cofactor (6.9), where CA is protonated, while its deprotonation at higher pH levels leads to the dissociation of the A-CA triplex into single A-strands and free CA cofactors. The structural transition is fully pH reversible. The A-CA triplex is further utilized as a crosslinking element for reprogrammable macroscopic object assembly, exemplified by hydrogel cubes (5 × 5 × 5 mm), a topic that has been less explored compared to nano- and microscopic constructs. Controlled, modular assembly and disassembly of various configurations, such as square, line, and T-shape, are demonstrated through reversible pH adjustments. This strategy offers a streamlined approach using a single DNA sequence and cofactor for hydrogel modification and complex construction, providing cost-effective, recyclable, and stimuli-responsive functionality, which inspires the development of versatile and adaptive supramolecular systems in chemistry and materials science.

Received 5th February 2025,
Accepted 21st March 2025

DOI: 10.1039/d5sm00124b

rsc.li/soft-matter-journal

Introduction

Supramolecular assembly represents an interesting and meaningful strategy for the controlled construction of functional frameworks.[1] Applications in diverse fields have been reported, including mimicking cells,[2] cell–cell communication,[3] constructing hierarchical surfaces,[4] aggregation-induced emission,[5,6] fluorescence modulators,[7] biological imaging,[8] light-harvesting systems,[9] *etc.* Notably, these advancements span nano- and microscale assemblies and have recently extended to meso- and macroscopic engineering, which has drawn considerable research interest.[10] Examples include underwater adhesion,[11,12] stereolithographic patterning,[13] multiple patterns,[14] data security,[15] self-propulsion systems,[16] multi-responsive hydrogels,[17] actuators,[18,19] *etc.* Achieving these applications relies on various supramolecular assembly strategies, such as host–guest recognition (cyclodextrin (CD)-adamantyl,[20] CD-azobenzene,[11] CD-ferrocene[13]), electrostatic attraction (polyethyleneimine (PEI)-polyacrylic acid (PAA),[21] PEI-gelatin,[22] poly(diallyldimethylammonium chloride)-(polystyrene sulfonate) (PDADMAC-PSS),[23] PAA-poly(allylamine hydrochloride) (PAH),[24] poly([2(methacryloyloxy)ethyl]trimethylammonium chloride)-poly(3-sulfopropyl methacrylate) (PMETAC-PSPMA),[12]), and dynamic covalent interaction (acylhydrazine–tetraaldehyde[14]). These strategies typically require the precise identification of two distinct components, necessitating the modification of one building block with one component and the other with its corresponding counter-component. Consequently, the recognition behaviour occurs exclusively in a sequential manner, following an ABAB⋯ pattern.

As a supramolecule in nature, DNA possesses numerous advantages, including programmability, designability, specific

[a] *Institute of Materials Research and Engineering (IMRE), Agency for Science, Technology and Research (A*STAR), 2 Fusionopolis Way, Innovis #08-03, 138634 Singapore, Republic of Singapore. E-mail: ywhu@imre.a-star.edu.sg*
[b] *College of Design and Engineering, National University of Singapore, 21 Lower Kent Ridge Road, 119077 Singapore, Republic of Singapore*
[c] *Department of Chemistry, National University of Singapore, 3 Science Drive 3, Singapore 117543, Republic of Singapore*
[d] *School of Interdisciplinary Studies, Lingnan University, Tuen Mun, Hong Kong SAR, China*
[e] *Science, Mathematics, and Technology (SMT), Singapore University of Technology and Design (SUTD), 8 Somapah Road, Singapore 487372, Republic of Singapore*

† Electronic supplementary information (ESI) available. See DOI: https://doi.org/10.1039/d5sm00124b

‡ These authors contributed equally.

Watson–Crick base-pairing, multiple stimuli-responsiveness, *etc.* These properties have enabled the development of various functional DNA constructs, such as origami,[25] superlattices,[26] hydrogels,[27] dynamic constitutional networks,[28] nano-assemblies,[29] nanomachines,[30] microcapsules,[31] molecular electronics,[32] logic gates,[33] and fibers,[34] with applications including computing,[35] data storage,[36] *etc.* Beyond nanoscale constructs, the structural characteristics and base-pairing (A-T, G-C) of DNA make it an ideal candidate for engineering meso- or macroscopic objects. Indeed, the assemblies of hydrogel cuboids through DNA recognition and binding have been developed. For example, hydrogel cuboids modified with rolling circle amplification-generated giant DNAs containing tandem repeated complementary sequences were assembled into multiple dimers.[37] Similarly, hydrogel cuboids modified with short DNA strands (25-mer[38] or 16-mer[39]) have been shown to form dimers *via* hybridization interaction between complementary sequences. However, these systems face challenges similar to those encountered in traditional supramolecular recognition. Specifically, they require the modification of macroscopic objects with two complementary components, leading to sequential recognition behaviour in an ABAB pattern. Additionally, the incorporation of diverse DNA sequences increases system complexity. Moreover, these DNA sequences generally lack responsiveness to external stimuli, limiting their utility in designing intelligent platforms that can adapt to environmental cues. A further challenge lies in achieving controlled assembly and disassembly of macroscopic objects in a random, non-sequential manner, akin to the versatility of LEGO® bricks.[40] Overcoming these limitations is crucial for advancing the field and enabling the creation of adaptable, responsive systems.

Herein, instead of using traditional Watson–Crick base-pairing derived recognition, we introduce low-molecular-weight cofactor mediated oligo-adenine triplexes as stimuli-responsive supramolecular configurations for the controlled assembly and disassembly of macroscopic objects. The cofactor, cyanuric acid (CA, pK_a 6.9), features three thymine-like faces (Fig. 1, right panel). At pH values below 6.9, the protonation of CA promotes the assembly of oligo-adenine (A21) into a supramolecular A-CA triplex, crosslinked by A-CA units. The A-CA unit adopts a helicene-like structure stabilized by Watson–Crick and Hoogsteen hydrogen bonding. Upon deprotonation at pH > 6.9, the A-CA triplex dissociates into single A21 strands and CA cofactors. The transitions are pH reversible. This cofactor CA-mediated assembly has been previously utilized to construct supramolecular fibers,[34,41,42] stimuli-responsive hydrogels,[43,44] DNA structures resistant to enzymatic degradation,[45] and other configurations.[46] Despite these advancements, the potential application of CA-mediated assembly in supramolecular DNA systems for macroscopic object construction has not yet been explored. Furthermore, this approach may potentially address the limitations encountered in traditional supramolecular recognition strategies, such as the reliance on sequential ABAB patterns and the lack of stimuli-responsiveness, thereby paving the way for more versatile and adaptive supramolecular systems.

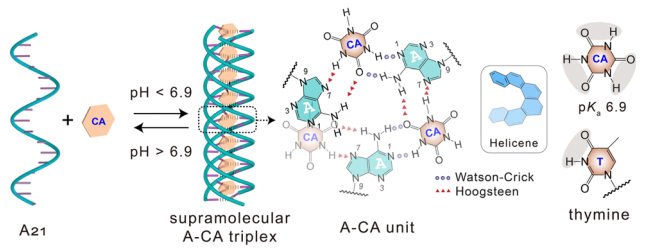

Fig. 1 Schematic representation of the CA-mediated supramolecular A-CA triplex, highlighting the pH-triggered, reversible assembly and disassembly process. The right panel illustrates the helicene-like structure of the A-CA unit framework, crosslinked through both Watson–Crick and Hoogsteen hydrogen bonding, alongside the thymine-like faces of CA.

Results and discussion

At pH 5, the A21 strands exhibit the characteristic behaviour of DNA, with a maximum absorbance at around λ_{260nm}, as depicted in Fig. 2A. Upon the introduction of CA cofactors to the A21 strands, a hypochromic effect was observed at λ_{260nm}, alongside a slight redshift, indicating an enhanced base-stacking interaction upon the generation of the A-CA triplex. Moreover, the rising of absorbance at λ_{285nm} was observed, a feature attributed to the generation of J-aggregates due to the stacking of ordered chromophores.[42,47] In contrast, these phenomena were absent at pH 8 (inset of Fig. 2A), indicating that the protonation of CA cofactors is essential for the formation of the A-CA triplex. Notably, no obvious absorbance peaks associated with CA cofactors were detected at these wavelengths.[44] The A-CA triplex, formed under mild acidic conditions, displays a well-defined sigmoidal shape with a melting temperature (T_m) of approximately 40 °C, as reported in previous studies.[34,44]

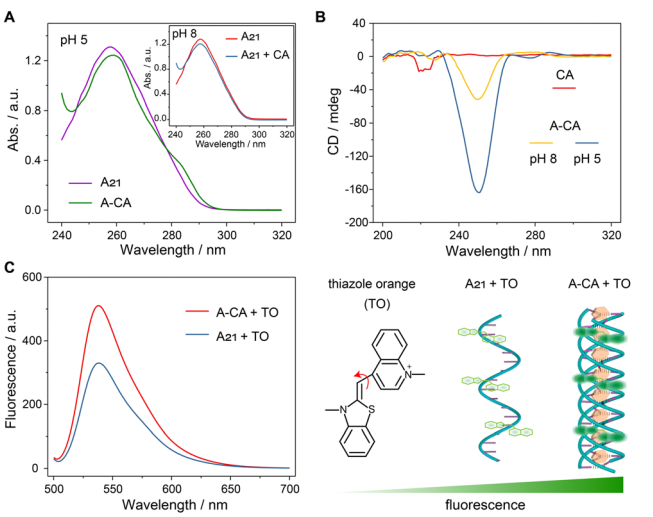

Fig. 2 (A) Absorbance spectra of A21 and A-CA at pH 5. (B) CD spectra of CA and A-CA at pH 8 and pH 5. (C) Fluorescence spectra of TO upon binding to the A-CA triplex and single A21 strands at pH 5. The molecular structures of TO, along with the schematic representations of TO binding to a single A21 strand and the A-CA triplex, accompanied by a fluorescence intensity indicator, are presented on the right panel.

Circular dichroism (CD) spectroscopy was adopted to further verify the formed A-CA triplex secondary structures at acidic pH value. As shown in Fig. 2B, a strong negative band peaking at λ_{250nm} is observed for the A-CA triplex at pH 5. However, the intensity of this band significantly diminishes at pH 8, a change attributed to the disassembly of the A-CA triplex caused by the deprotonation of CA cofactors. These results are consistent with previous studies,[34,42] demonstrating that CA cofactors mediate the assembly of A21 strands into a helicene-like A-CA triplex structure through both Watson–Crick and Hoogsteen interactions. In the A-CA configuration, the stoichiometry of CA cofactors to adenine bases was determined to be 1, consistent with a 1 : 1 CA : adenine ratio in the helicene-like structure.[42] Notably, in the absence of CA cofactors, A21 strands exhibited similar CD spectra at pH 5 and pH 8 (Fig. S1, ESI†). Additionally, no characteristic CD peaks corresponding to CA cofactors were observed (Fig. 2B).

To further differentiate between the A-CA triplex and single A21 strands, a fluorescent indicator, thiazole orange (TO), was employed. TO is an asymmetric cyanine molecule composed of conjugated benzothiazole and quinoline aromatic rings linked with a single methine bond. (Fig. 2C). The free intramolecular rotation of TO along the methine bond leads to a nonradiative decay of its excited state, resulting in negligible fluorescence (Fig. S2, ESI†). However, when TO molecules bind to rigid DNA duplexes, a 10^3-fold enhancement of fluorescence was reported.[48,49] Similarly, a substantial increase in TO fluorescence was detected upon its binding to the A-CA triplex at pH 5 (Fig. 2C). This enhancement is attributed to the intercalation or stacking of TO molecules within the helicene-like structure of the A-CA triplex. The rigid A-CA triplex restricts the torsional motion and maintains the planarity of TO, resulting in higher fluorescence compared to TO binding with single A21 strands, which exhibit random flexible coils in solution. The greater flexibility of single A21 strands imposes fewer restrictions on the free rotation of TO molecules, resulting in lower fluorescence. While at pH 8, nearly identical fluorescence behaviour of TO was observed for A21 strands, regardless of the presence or absence of CA cofactors (Fig. S3, ESI†). These results confirm that the protonation of CA cofactors is a prerequisite to generate A-CA triplex configurations. Notably, neither CA cofactors alone nor the mixture of TO with CA exhibited detectable fluorescence (Fig. S2, ESI†).

After confirming that protonated CA cofactors induce the formation of A-CA triplexes, we further investigated the strand orientation of A21 within these configurations. Previous studies using CD spectra and thermal denaturation have established the parallel orientation of A-strands in A-CA triplexes.[42] Herein, pyrene (Py)-modified A21 strands (Py-A21) were employed to explore the strand orientation further. Py is a fluorophore with spatial sensitivity, which exhibits aggregation-induced emission (AIE) upon the formation of excimers *via* π–π stacking.[50,51] As demonstrated in Fig. 3A, Py-A21 strands exist as single coils with Py in the monomeric state at pH 8, even in the presence of CA cofactors. However, upon changing the system pH value to 5, CA cofactors mediate the formation of

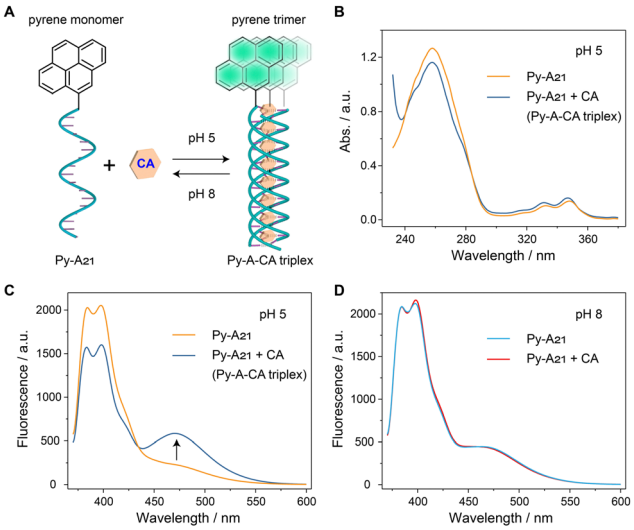

Fig. 3 (A) Schematic demonstration of the CA-mediated assembly of single Py-A21 strands into a Py-A-CA triplex, exhibiting fluorescence at λ_{470nm} generated by the pyrene trimer. (B) Absorbance spectra and (C) fluorescence spectra of Py-A21 and the CA-mediated Py-A-CA triplex at pH 5. (D) Fluorescence spectra of Py-A21 with and without CA cofactors at pH 8.

the Py-A-CA triplex, resulting in the close proximity of Py monomers and the formation of Py excimers (Fig. 3A). At pH 5, Py-A21 strands display the characteristic absorbance peaks of DNA (λ_{260nm}) and Py (λ_{330nm}, λ_{346nm}) (Fig. 3B). With the introduction of CA cofactors, a hypochromic effect was also observed at λ_{260nm}, consistent with the formation of the A-CA triplex (Fig. 2A). In contrast, no such absorbance changes were observed at pH 8 (Fig. S4, ESI†). These results show that the modification of Py at the 5′-terminal of A21 does not impede the efficient assembly of Py-A21 strands into Py-A-CA triplexes.

As depicted in Fig. 3C, Py-A21 strands exhibit the characteristic fluorescence peaks of Py monomers at λ_{384nm} and λ_{398nm} in the absence of CA cofactors at pH 5. Upon the introduction of CA cofactors, a new Py excimer emission peak at λ_{470nm} emerged, accompanied by a decrease in fluorescence intensity at λ_{384nm} and λ_{398nm}. This appearance of the Py excimer peak confirms the parallel strand orientation in the Py-A-CA triplexes, which facilitates the stacking of Py monomers. While at pH 8, Py-A21 strands remained as single random coils, regardless of the absence or presence of CA cofactors, as indicated by the fluorescence of Py monomers (Fig. 3D).

As an example of macroscopic object assembly, hydrogel cubes with dimensions of 5 × 5 × 5 mm were first prepared. As depicted in Fig. 4A, the chemical ingredients including acrylamide (AA)/bis-acrylamide (BIS), acrylamide-polyethylene glycol-azide (ACA-PEG-N_3) and deoxyribonucleic acid sodium salt from salmon testes (DNAss) were copolymerized in custom cube molds *via* free radical polymerization with ammonium persulfate (APS) and *N*,*N*,*N*′,*N*′-tetramethylethylenediamine (TEMED) as the initiator/accelerator. The as-prepared hydrogel cubes were opaque (cube-o, Fig. 4B), due to the incorporation of ACA-PEG-N_3, which introduced azide functional groups on the

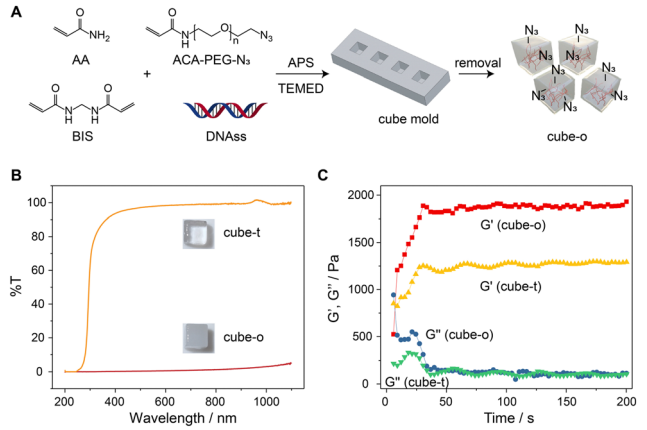

Fig. 4 (A) Schematic representation of the synthesis of hydrogel cubes. (B) Transmittance and (C) rheology measurements of hydrogel cubes prepared with (cube-o) and without (cube-t) ACA-PEG-N_3.

cube surfaces, facilitating the subsequent modification with DNA strands. Without the addition of ACA-PEG-N_3, the prepared cubes are transparent (cube-t, Fig. 4B), which exhibit a significant decrease in transmittance in the UV region. Rheology measurements also distinguished the two types of hydrogel cubes, with the storage modulus (G') value of cube-o ($G' \approx 1850$ Pa) being much higher than that of cube-t ($G' \approx 1250$ Pa) (Fig. 4C). This result demonstrates that the incorporation of ACA-PEG-N_3 into the hydrogel cubes introduced additional polymer chains, resulting in a more rigid structure.

To differentiate the hydrogel cubes, fluorescent DNA intercalators, such as DAPI, GelRed, SYBR Safe, and SYBR Gold, were used to stain these cubes, which exhibited fluorescence under UV light irradiation (λ_{365nm}). This fluorescence was a result of the intercalation of these dyes to double-stranded DNAss within the hydrogel cubes. To facilitate the linkage of A21 strands onto the surfaces of hydrogel cubes with azide functional groups, 5′-terminal dibenzocyclooctyne modified A21 (DBCO-A21) strands were employed. Using the strain-promoted azide–alkyne [3+2] cycloaddition (SPAAC), which is a widely adopted orthogonal interaction in biochemistry, A21 strands were attached to the surfaces of hydrogel cubes (Fig. 5A). The attached average amount of DBCO-A21 onto each hydrogel cube was calculated to be ≈ 3.9 nmol, determined by subtracting the amount of unbound DBCO-A21 remaining in the buffer solution after incubation from the initial amount added. As shown in the scanning electron microscopy image (Fig. S5, ESI†), the surface morphology of the hydrogel cubes exhibited no obvious change after the conjugation of DBCO-A21 strands.

With the introduction of CA cofactors at pH 5, the formation of supramolecular A-CA triplexes bridges the macroscopic hydrogel cubes into desired configurations. When the pH value was adjusted to 8, the deprotonation of CA cofactors resulted in the dissociation of the A-CA triplex bridges into A21 single strands and free CA cofactors and consequently the

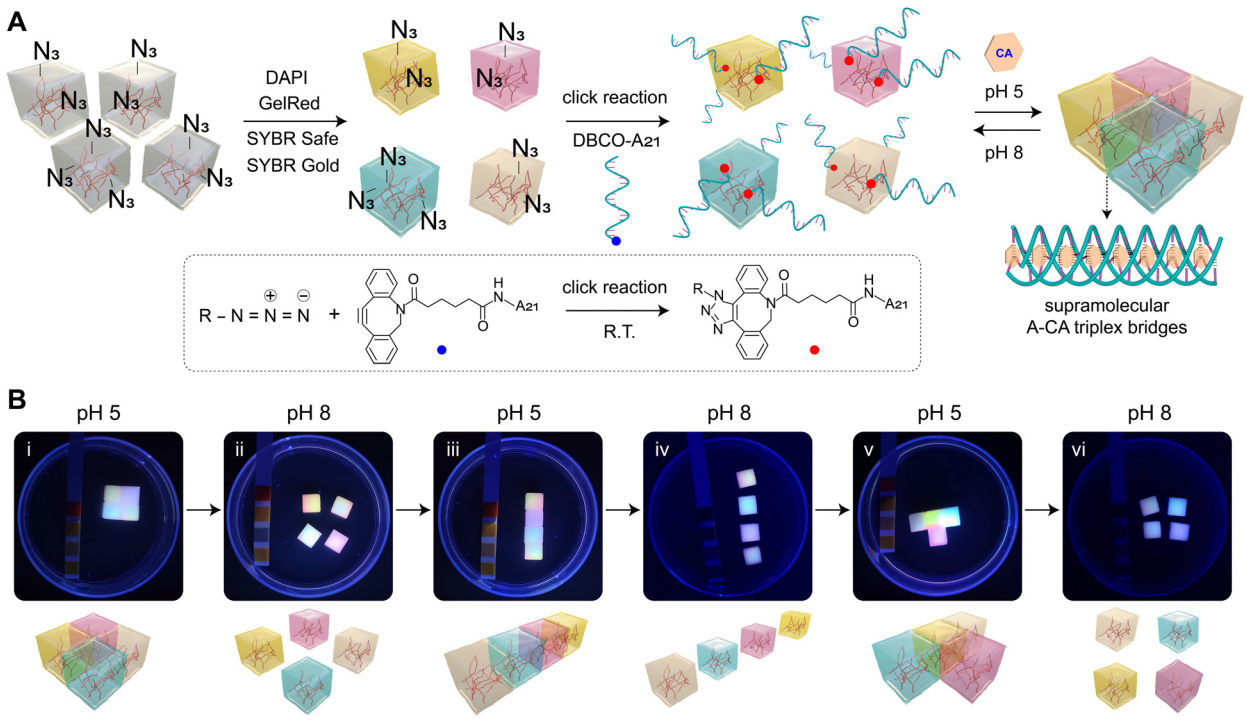

Fig. 5 (A) Schematic representation of preparing fluorescent dye-stained hydrogel cubes, followed by modification with DBCO-A21 *via* a click reaction (SPAAC, dashed box). At pH 5 and with CA cofactors, the generation of supramolecular A-CA triplex bridges facilitates the assembly of macroscopic hydrogel cubes into desired architectures, which disassemble upon adjusting the system pH to 8. (B) Photographs showcasing the assembly of hydrogel cubes into various architectures at pH 5 and their disassembly at pH 8. The dimensions of the hydrogel cubes are 5 × 5 × 5 mm. The images were taken under UV light (365 nm).

deconstruction of the macroscopic structures (Fig. 5A). This process is trigger-reversible, resembling the construction and deconstruction of LEGO® bricks. As exemplified in panel i (Fig. 5B), a square shape consisting of four hydrogel cubes was assembled in a Petri at pH 5 (a pH indicator paper was inserted to demonstrate the pH value). A video showing the movement of the assembled macroscopic structure is provided (Video S1, ESI†). When the system pH was adjusted to 8, the square shape disassembled into single hydrogel cubes (panel ii, Video S2, ESI†). Reconfiguration of the hydrogel cubes into a linear shape was achieved at pH 5 (panel iii, Video S3, ESI†), and upon adjusting the pH to 8, the structure disassembled into single cubes again (panel iv, Video S4, ESI†). A reassembled T-shape structure was subsequently demonstrated at pH 5 (panel v, Video S5, ESI†), which reverted to single cubes at pH 8 (panel vi, Video S6, ESI†). The observed color loss in panel vi might be attributed to photobleaching caused by prolonged exposure to UV irradiation. To provide a clearer comparison, an enlarged version of panel vi, highlighting the differences, has been included as Fig. S6 in the ESI.† Theoretically, the assembly and disassembly of these hydrogel cubes could be recycled multiple times, much like LEGO® toys. However, during the reconstruction processes, potential damage to the A21 strands attached on the surfaces of hydrogel cubes might lead to reduced assembly efficiency. By exploiting CA cofactors mediated supramolecular DNA configurations in the controlled assembly and disassembly of macroscopic objects, several merits are desirable. For example, unlike previous studies that require at least two complementary DNA sequences to modify two hydrogel cubes,[38,39] only one DNA sequence is required in this study, simplifying the modification process. Moreover, the pH-triggered A-CA triplex bridges enable the responsiveness of the constructs to external stimuli. This pH-reversibility enhances cost-effectiveness, simplicity, and recyclability, which are not typically present in complementary DNA strand-based systems.[38,39] Additionally, unlike the sequential ABAB$\cdots$ pattern assembly of one block and its counterpart, the current method allows for arbitrary and reprogrammable construction of hydrogel cubes through CA cofactor-mediated supramolecular A-CA triplexes.

Conclusion

In summary, cyanuric acid (CA), a low-molecular-weight cofactor bearing thymine-like edges, facilitates the assembly of adenine-rich strands (A-strands) into a supramolecular A-CA triplex structure. Involving both Watson–Crick and Hoogsteen interactions, the noncanonical A-CA triplex resembles a helicene configuration. Spectroscopic studies demonstrated the formation and dissociation of the A-CA triplex at pH 5 and pH 8, respectively, corresponding to the protonation and deprotonation of CA cofactors (pK_a 6.9). The parallel orientation of the strands was further investigated by using a spatially sensitive fluorophore, pyrene, modified A-strands, which exhibited the pyrene excimer fluorescence upon aggregation-induced emission in the assembled A-CA triplex. Moreover, the pH-responsive noncanonical A-CA triplex was developed as a cross-linking element for the reprogrammable assembly of macroscopic objects (hydrogel cubes with the dimensions of 5 × 5 × 5 mm). The controlled, modular assembly and disassembly of various configurations, including square, line and T-shape, were successfully demonstrated. And the merits of exploiting the CA cofactor-mediated A-CA triplex for macroscopic object assembly were also discussed, highlighting their superiority over conventional assembly strategies. Inspired by this study, future advancements in cofactor-mediated DNA conformations in nano/micro-object construction, drug release, nanomachines and structured materials can be envisaged. By leveraging artificial intelligence and machine learning based techniques, the discovery and investigation of new cofactors and their functions in mediating noncanonical DNA structures could lead to exciting innovations in the field and beyond.

Author contributions

Y. H. conceived and designed the research. A. Z. T. L., M. S. M. H., Y. K. and W. W. L. performed experiments and collected data. Z. D., F. W., J. Y. C. L., X. T. Z., L. Y. and Y. H. performed formal analysis. Y. H. wrote the manuscript with input from all authors.

Data availability

The experimental details supporting this article are available in the ESI.†

Conflicts of interest

There are no conflicts to declare.

Acknowledgements

The research is supported by the Career Development Fund (C210112014), SERC Central Research Fund (CRF, UIBR, KIM-R220901aSERCRF), and RIE2025 Manufacturing, Trade, and Connectivity (MTC) Programmatic Fund under grant M24M 9b0013 entitled BLISS: Beyond Liquids with *In-Situ* Solid-state Surficial Sensorics, IMRE, A*STAR, Singapore. The kind assistance with the SEM by Karen Tang Yuanting is greatly appreciated.

References

1 T. Aida, E. W. Meijer and S. I. Stupp, *Science*, 2012, **335**, 813–817.
2 Y. Tu, F. Peng, A. Adawy, Y. Men, L. K. Abdelmohsen and D. A. Wilson, *Chem. Rev.*, 2016, **116**, 2023–2078.
3 P. Shi, E. Ju, Z. Yan, N. Gao, J. Wang, J. Hou, Y. Zhang, J. Ren and X. Qu, *Nat. Commun.*, 2016, **7**, 13088.

4 D. P. Goronzy, M. Ebrahimi, F. Rosei Arramel, Y. Fang, S. De Feyter, S. L. Tait, C. Wang, P. H. Beton, A. T. S. Wee, P. S. Weiss and D. F. Perepichka, *ACS Nano*, 2018, **12**, 7445–7481.
5 X. Y. Lou and Y. W. Yang, *Aggregate*, 2020, **1**, 19–30.
6 N. Song, Z. Zhang, P. Liu, Y. W. Yang, L. Wang, D. Wang and B. Z. Tang, *Adv. Mater.*, 2020, **32**, e2004208.
7 X. M. Chen, X. F. Hou, H. K. Bisoyi, W. J. Feng, Q. Cao, S. Huang, H. Yang, D. Chen and Q. Li, *Nat. Commun.*, 2021, **12**, 4993.
8 W. L. Zhou, W. Lin, Y. Chen and Y. Liu, *Chem. Sci.*, 2022, **13**, 7976–7989.
9 K. Wang, K. Velmurugan, B. Li and X. Y. Hu, *Chem. Commun.*, 2021, **57**, 13641–13654.
10 M. Cheng and F. Shi, *Chem. – Eur. J.*, 2020, **26**, 15763–15778.
11 G. Ju, M. Cheng, F. Guo, Q. Zhang and F. Shi, *Angew. Chem., Int. Ed.*, 2018, **57**, 8963–8967.
12 C. Lin, F. Hou, Q. Zhang, G. Zhu, M. Cheng and F. Shi, *Small*, 2024, **20**, e2404526.
13 A. Keutgen, I. Klein, F. Shi and A. J. C. Kuehne, *Adv. Funct. Mater.*, 2023, **34**, 2310835.
14 X. Ji, Z. Li, X. Liu, H. Q. Peng, F. Song, J. Qi, J. W. Y. Lam, L. Long, J. L. Sessler and B. Z. Tang, *Adv. Mater.*, 2019, **31**, e1902365.
15 Y. Zhang, X. Le, Y. Jian, W. Lu, J. Zhang and T. Chen, *Adv. Funct. Mater.*, 2019, **29**, 1905514.
16 G. Lu, G. Zhu, Q. Zhang, P. Tian, M. Cheng and F. Shi, *Angew. Chem., Int. Ed.*, 2023, **62**, e202300448.
17 C. Ma, T. Li, Q. Zhao, X. Yang, J. Wu, Y. Luo and T. Xie, *Adv. Mater.*, 2014, **26**, 5665–5669.
18 W. Lu, R. Wang, M. Si, Y. Zhang, S. Wu, N. Zhu, W. Wang and T. Chen, *SmartMat*, 2024, **5**, e1190.
19 R. Baretta, G. Davidson-Rozenfeld, V. Gutkin, M. Frasconi and I. Willner, *J. Am. Chem. Soc.*, 2024, **146**, 9957–9966.
20 A. Harada, R. Kobayashi, Y. Takashima, A. Hashidzume and H. Yamaguchi, *Nat. Chem.*, 2011, **3**, 34–37.
21 G. Ju, F. Guo, Q. Zhang, A. J. C. Kuehne, S. Cui, M. Cheng and F. Shi, *Adv. Mater.*, 2017, **29**, 1702444.
22 Y. Xue, K. Ye, X. Wang, Y. Xiang, S. Pang, C. Bao and L. Zhu, *Chem. Commun.*, 2021, **57**, 8786–8789.
23 M. Tan, P. Tian, Q. Zhang, G. Zhu, Y. Liu, M. Cheng and F. Shi, *Nat. Commun.*, 2022, **13**, 5201.
24 Q. Zhang, B. Zhao, Z. Lin, F. Shi and M. Cheng, *ACS Appl. Mater. Interfaces*, 2023, **15**, 2459–2467.
25 P. Zhan, A. Peil, Q. Jiang, D. Wang, S. Mousavi, Q. Xiong, Q. Shen, Y. Shang, B. Ding, C. Lin, Y. Ke and N. Liu, *Chem. Rev.*, 2023, **123**, 3976–4050.
26 Q. Y. Lin, J. A. Mason, Z. Li, W. Zhou, M. N. O'Brien, K. A. Brown, M. R. Jones, S. Butun, B. Lee, V. P. Dravid, K. Aydin and C. A. Mirkin, *Science*, 2018, **359**, 669–672.
27 J. S. Kahn, Y. Hu and I. Willner, *Acc. Chem. Res.*, 2017, **50**, 680–690.
28 L. Yue, S. Wang, Z. Zhou and I. Willner, *J. Am. Chem. Soc.*, 2020, **142**, 21577–21594.
29 G. Yao, J. Li, Q. Li, X. Chen, X. Liu, F. Wang, Z. Qu, Z. Ge, R. P. Narayanan, D. Williams, H. Pei, X. Zuo, L. Wang, H. Yan, B. L. Feringa and C. Fan, *Nat. Mater.*, 2020, **19**, 781–788.
30 D. Y. Zhang and G. Seelig, *Nat. Chem.*, 2011, **3**, 103–113.
31 A. Fischer, S. Lilienthal, M. Vazquez-Gonzalez, M. Fadeev, Y. S. Sohn, R. Nechushtai and I. Willner, *J. Am. Chem. Soc.*, 2020, **142**, 4223–4234.
32 C. Guo, K. Wang, E. Zerah-Harush, J. Hamill, B. Wang, Y. Dubi and B. Xu, *Nat. Chem.*, 2016, **8**, 484–490.
33 A. Okamoto, K. Tanaka and I. Saito, *J. Am. Chem. Soc.*, 2004, **126**, 9458–9463.
34 F. J. Rizzuto, C. M. Platnich, X. Luo, Y. Shen, M. D. Dore, C. Lachance-Brais, A. Guarne, G. Cosa and H. F. Sleiman, *Nat. Chem.*, 2021, **13**, 843–849.
35 H. Lv, N. Xie, M. Li, M. Dong, C. Sun, Q. Zhang, L. Zhao, J. Li, X. Zuo, H. Chen, F. Wang and C. Fan, *Nature*, 2023, **622**, 292–300.
36 L. Organick, S. D. Ang, Y. J. Chen, R. Lopez, S. Yekhanin, K. Makarychev, M. Z. Racz, G. Kamath, P. Gopalan, B. Nguyen, C. N. Takahashi, S. Newman, H. Y. Parker, C. Rashtchian, K. Stewart, G. Gupta, R. Carlson, J. Mulligan, D. Carmean, G. Seelig, L. Ceze and K. Strauss, *Nat. Biotechnol.*, 2018, **36**, 242–248.
37 H. Qi, M. Ghodousi, Y. Du, C. Grun, H. Bae, P. Yin and A. Khademhosseini, *Nat. Commun.*, 2013, **4**, 2275.
38 V. A. Sontakke and Y. Yokobayashi, *J. Am. Chem. Soc.*, 2022, **144**, 2149–2155.
39 M. Nakahata, Y. Takashima, A. Hashidzume and A. Harada, *Chem. – Eur. J.*, 2015, **21**, 2770–2774.
40 E. Boulter, J. Colombelli, R. Henriques and C. C. Feral, *Trends Biotechnol.*, 2022, **40**, 1073–1087.
41 C. Lachance-Brais, C. D. Hennecker, A. Alenaizan, X. Luo, V. Toader, M. Taing, C. D. Sherrill, A. K. Mittermaier and H. F. Sleiman, *J. Am. Chem. Soc.*, 2021, **143**, 19824–19833.
42 N. Avakyan, A. A. Greschner, F. Aldaye, C. J. Serpell, V. Toader, A. Petitjean and H. F. Sleiman, *Nat. Chem.*, 2016, **8**, 368–376.
43 C. Lachance-Brais, M. Rammal, J. Asohan, A. Katolik, X. Luo, D. Saliba, A. Jonderian, M. J. Damha, M. J. Harrington and H. F. Sleiman, *Adv. Sci.*, 2023, **10**, e2205713.
44 Y. Hu, J. Liu, Y. Ke, B. Wang, J. Y. C. Lim, Z. Dong, Y. Long and I. Willner, *ACS Appl. Mater. Interfaces*, 2024, **16**, 29235–29247.
45 C. Lachance-Brais, C. Yao, A. Reyes-Valenzuela, J. Asohan, E. Guettler and H. F. Sleiman, *J. Am. Chem. Soc.*, 2024, **146**, 5811–5822.
46 Y. Hu and I. Willner, *Angew. Chem., Int. Ed.*, 2024, **63**, e202412106.
47 E. E. Jelley, *Nature*, 1936, **138**, 1009–1010.
48 J. Nygren, N. Svanvik and M. Kubista, *Biopolymers*, 1998, **46**, 39–51.
49 F. Hovelmann and O. Seitz, *Acc. Chem. Res.*, 2016, **49**, 714–723.
50 X. Feng, X. Wang, C. Redshaw and B. Z. Tang, *Chem. Soc. Rev.*, 2023, **52**, 6715–6753.
51 J. Huang, Y. Wu, Y. Chen, Z. Zhu, X. Yang, C. J. Yang, K. Wang and W. Tan, *Angew. Chem., Int. Ed.*, 2011, **50**, 401–404.

